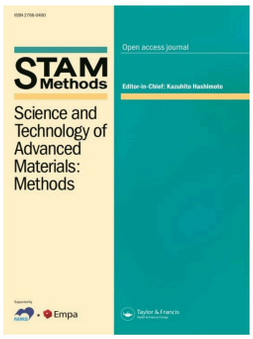

Taylor & Francis
Taylor & Francis Group

Science and Technology of Advanced Materials: Methods

ISSN: 2766-0400 (Online) Journal homepage: www.tandfonline.com/journals/tstm20

Enhancing thermoelectric efficiency of GeTe through process improvement via active learning assisted by Bayesian optimisation

Florent Pawula, Mathias Hamitouche, Linda Abbassi, Agathe Bajan, Cédric Bourgès, Takao Mori, Jean-François Halet, David Berthebaud & Guillaume Lambard

To cite this article: Florent Pawula, Mathias Hamitouche, Linda Abbassi, Agathe Bajan, Cédric Bourgès, Takao Mori, Jean-François Halet, David Berthebaud & Guillaume Lambard (2025) Enhancing thermoelectric efficiency of GeTe through process improvement via active learning assisted by Bayesian optimisation, Science and Technology of Advanced Materials: Methods, 5:1, 2545174, DOI: 10.1080/27660400.2025.2545174

To link to this article: https://doi.org/10.1080/27660400.2025.2545174

SCIENCE AND TECHNOLOGY OF ADVANCED MATERIALS: METHODS
2025, VOL. 5, NO. 1, 2545174
https://doi.org/10.1080/27660400.2025.2545174

Enhancing thermoelectric efficiency of GeTe through process improvement via active learning assisted by Bayesian optimisation

Florent Pawula[a,b,c], Mathias Hamitouche[b,d], Linda Abbassi[b,d], Agathe Bajan[a], Cédric Bourgès[d], Takao Mori[d], Jean-François Halet[b,e], David Berthebaud[b,c] and Guillaume Lambard[a,b]

[a]Data-driven materials design group, Center for Basic Research on Materials (CBRM), National Institute for Materials Science (NIMS), Tsukuba, Ibaraki, Japan; [b]CNRS-Saint Gobain-NIMS, IRL 3629, Laboratory for Innovative Key Materials and Structures (LINK), National Institute for Materials Science (NIMS), Tsukuba, Ibaraki, Japan; [c]Nantes Université, CNRS, Institut des Matériaux de Nantes Jean Rouxel, IMN, Nantes, France; [d]Thermal Energy Group, WPI International Center for Materials Nanoarchitectonics (WPI-MANA), National Institute for Materials Science (NIMS), Tsukuba, Japan; [e]Univ Rennes, CNRS, Ecole Nationale Supérieure de Chimie de Rennes (ENSCR), Institut des Sciences Chimiques de Rennes (ISCR), Rennes, France

ABSTRACT

Pristine GeTe is an archetypal mid-temperature thermoelectric, but its full potential is obscured by an eleven-dimensional process space. We combine active learning with Bayesian optimisation (ALBO) to traverse this landscape, encompassing melt-annealing and spark-plasma-sintering conditions. Starting from five random experiments, ALBO iteratively proposes batches of five new recipes by maximising the expected improvement in the figure-of-merit zT; each batch is synthesised, characterised, and used to retrain the surrogate. After only 24 experiments – four orders of magnitude fewer than an exhaustive search – we raise the 700 K zT of undoped GeTe from 0.86 to 1.14, a 25% gain over the best conventional two-step route and comparable to multi-day three-step protocols. Post-hoc analysis reveals that melt-cooling rate and SPS dwell/cooling profiles dominate performance by controlling the Ge-vacancy population and microstructure. ALBO therefore provides a time- and energy-efficient path to process optimisation while simultaneously exposing the key levers that govern transport in GeTe, and the strategy is readily transferable to other materials where processing, rather than chemistry, limits performance.

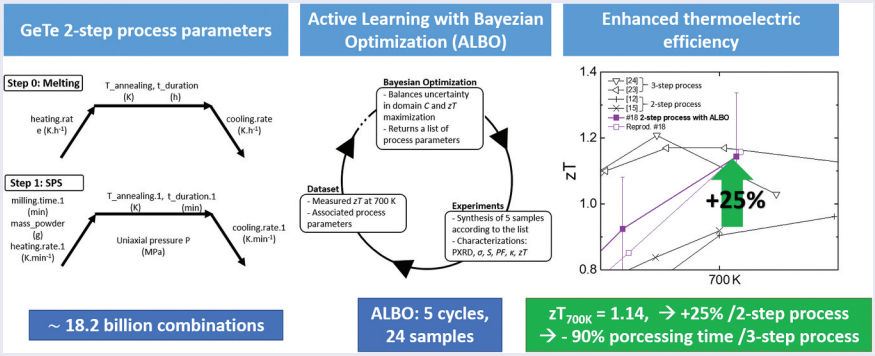

IMPACT STATEMENT

This study pioneers AI-assisted full-process optimisation of bulk materials, improving the targeted property while reducing experimentation from billion of possibilities to 24 trials, highlighting our method transformative potential in materials processing.

ARTICLE HISTORY
Received 16 April 2025
Revised 29 July 2025
Accepted 4 August 2025

KEYWORDS
Material process; bayesian optimisation; active learning; chalcogenides; thermoelectrics

1. Introduction

Germanium telluride (GeTe) is one of the most promising IV-VI chalcogenides for mid-temperature power generation (~500-800 K) because it can reach a dimensionless figure-of-merit of $zT = \sigma S^2 T/\kappa$, where σ is the electrical conductivity (S m^{-1}), S is the Seebeck coefficient (V K^{-1}), T is the absolute temperature (K), and κ is the thermal conductivity (W m^{-1} K^{-1}), close to unity. Its favourable electronic term (σS^2) stems from an intrinsically high hole concentration (10^{20}–10^{21} cm^{-3}) created by Ge vacancies, which persists across the rhombohedral-to-cubic transition that occurs at about 700 K [1,2]. Above this

CONTACT Guillaume Lambard LAMBARD.Guillaume@nims.go.jp Data-driven materials design group, Center for Basic Research on Materials (CBRM), National Institute for Materials Science (NIMS), Tsukuba, Ibaraki, Japan; Florent Pawula florent.pawula@cnrs-imn.fr Nantes Université, CNRS, Institut des Matériaux de Nantes Jean Rouxel, IMN, Nantes, France
Supplemental data for this article can be accessed online at https://doi.org/10.1080/27660400.2025.2545174

temperature, the slight trigonal distortion vanishes and the lattice becomes an ideal rocksalt, but the defect chemistry, and hence the *p*-type conductivity, remains essentially unchanged.

The main obstacle to further increasing the thermoelectric figure-of-merit zT is the lattice's relatively large thermal conductivity ($\kappa \approx 3-4$ W.m^{-1}.K^{-1} [3]), which suppresses zT. Conventional approaches therefore focus on (i) tuning carrier concentration by Sb/Bi alloying to raise S without sacrificing σ [4,5]; and (ii) introducing point defects, secondary phases, or nanostructures to scatter phonons and lower κ [6]. Despite these efforts, pristine GeTe still struggles with the competing requirements of low κ and high σ, with simultaneously a reasonably large Seebeck coefficient S to keep the power factor P$F = \sigma S^2$ high [7].

Over the past decade, artificial-intelligence workflows, chiefly active learning combined with Bayesian optimisation (ALBO), have transformed the pace at which new functional materials are discovered and refined [8,9]. In a typical ALBO loop, an initial data set is used to train a surrogate model that predicts target physicochemical properties; an acquisition function then nominates the next experiments to be performed in the laboratory; the resulting data are added to the training set; and the cycle is repeated, progressively guiding the search through a high-dimensional design space toward an optimum material possessing targeted properties [10]. Because each cycle exploits what is already known while exploring the most informative unknowns, ALBO can pinpoint favourable process windows with an order of magnitude fewer experiments than conventional design-of-experiments protocols [11].

Pristine GeTe provides an ideal test bed for this strategy. The compound is normally fabricated either by a two-step or a three-step route. In the shorter two-step process, a Ge-Te melt (1000–1300 K for 1–12 h) is quenched, after which the ingot is densified by spark-plasma sintering or hot pressing (750–900 K for 5–60 min under 30–85 MPa) [12–18]. The longer three-step protocol inserts an additional 900 K anneal of 3–5 days before densification [19–25]. Our goal is to raise the figure-of-merit zT of undoped GeTe by optimising only the two-step parameters, thereby avoiding chemical alloying or deliberately engineered nanostructures. To that end we define an eleven-dimensional search space comprising all process variables accessible in a standard laboratory. Bayesian optimisation proposes the most informative combination for each new run, while active learning retrains the surrogate model after every batch, so the campaign rapidly alternates between probing completely new regions (exploration) and fine-tuning the most promising ones (exploitation) [26]. Similar ALBO protocols have already proved effective for catalysts [27], battery electrolytes [28], and, most pertinently, a sulfide thermoelectric in which the figure-of-merit was boosted from 0.27 to 0.36 at 675 K in only four cycles of ALBO, each cycle comprised of 6–7 newly proposed experiments [29]. By transferring this framework to GeTe we target the concurrent enhancement of the power factor P$F = \sigma S^2$ and the suppression of the thermal conductivity κ, thereby maximising zT. The results presented below confirm that ALBO can navigate the 11-parameter landscape with just a few dozen experiments and deliver swift, data-efficient gains in pristine GeTe, underscoring the broad applicability of AI-assisted process optimisation across thermoelectric materials.

2. Methods

2.1. Synthesis and process

High-purity Ge ingots (99.999%) and Te shots (99.999%, Rare Metallic Co. Ltd.) were weighed to a nominal 1:1 atomic ratio, loaded into 12 mm-diameter quartz ampoules and flame-sealed under primary vacuum ($\simeq 10^{-3}$ mbar). Each ampoule was heated to the a selected temperature, $T_{annealing}$ (1000–1300 K), for a $t_{duration}$ (1–12 h) at a programmable heating rate, *heating_rate* (10–150 K.h^{-1}), held, and either furnace-cooled or water-quenched according to the scheduled cooling rate *cooling_rate* (25–150 K.h^{-1}).

The solidified ingots were ground manually in an agate mortar for a time $t_{milling.1}$ (2–15 min) and a mass of powder, *mass_powder* (4–6 g), were loaded into a 10 mm graphite die lined with graphite paper to avoid sticking and carbon pick-up during sintering [30]. Densification was carried out by spark-plasma sintering (SPS, Dr. Sinter 1080) at a temperature $T_{annealing.1}$ (700–950 K) for a duration $t_{duration.1}$ (0–30 min), under an axial pressure P (40–70 MPa), and at a heating and cooling rate, $heating_{rate.1}$ and $cooling_{rate.1}$ (25–200 K.min^{-1}), respectively. The chamber was back-filled with Ar to 0.05 MPa for the entire run.

Figure 1a summarises the melting and SPS phases of synthesis and process of GeTe samples. Additionally, the full set of process parameters considered for optimisation of the zT under ALBO, together with their discretisation, is compiled in Table 1.

2.2. Characterisation

Cylindrical compacts were sectioned into bars ($\approx 2 \times 2 \times 8$ mm^3) and discs ($\emptyset \approx 10$ mm, 2 mm thick) and polished to a 1 μm finish prior to measurement. Phase purity was verified by powder X-ray diffraction (Rigaku MiniFlex 3, Cu Kα radiation) over

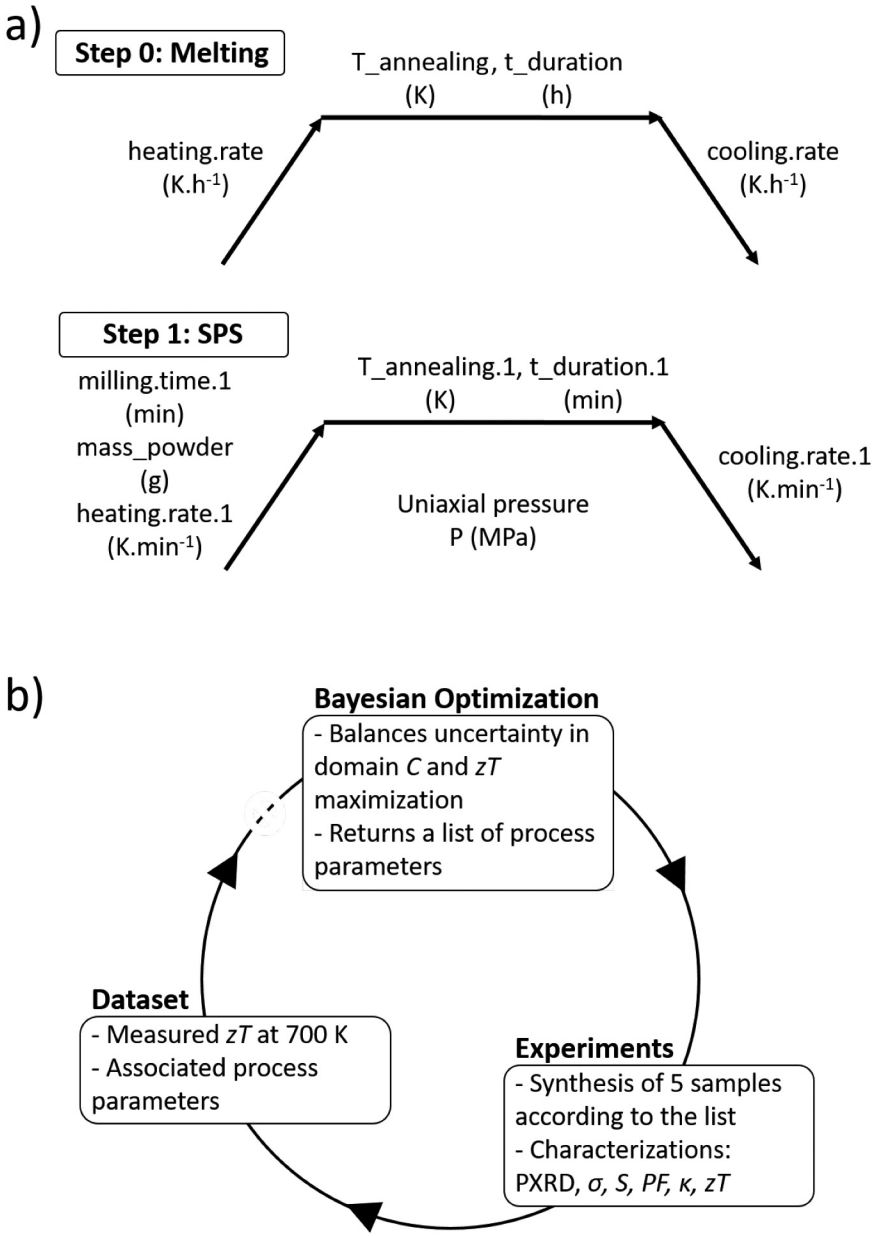

Figure 1. (a) process scheme with the associated process parameters (see table 1 for discretisation). (b) active learning scheme for optimisation of process parameters for improving *zT* values using Bayesian optimisation. The first cycle (starting point represented by the dotted line) consisted of 5 random proposals of process parameters (see table 1) constrained within the discretised domain *C*. The following cycles were performed on process parameters proposed via BO based on the dataset built from all the previous ALBO cycles.

Table 1. Discretisation of domain *C* with the associated resolution Δ.

Process parameter	min	max	Δ	unit
T annealing	1023	1473	25	K
t duration	0.1	24	2	h
heating rate	10	150	10	$K.h^{-1}$
cooling rate	25	150	25	$K.h^{-1}$
milling time.1	2	15	1	min
mass powder	4	6	0.25	g
T annealing.1	700	950	50	K
t duration.1	0	30	5	min
heating rate.1	25	200	25	$K.min^{-1}$
cooling rate.1	25	200	25	$K.min^{-1}$
P	40	70	5	MPa

$10° \leq 2\theta \leq 90°$ (step 0.02°, 10° min^{-1}). Le Bail refinements were performed with FULLPROF/WinPLOTR [31] using a pseudo-Voigt profile and Legendre background.

Electrical resistivity and Seebeck coefficient were measured simultaneously between 300 K and 700 K on a ULVAC-Riko ZEM-3 following the round-robin protocol of Bochmann *et al.* [32]. Thermal diffusivity $D(T)$ was determined on graphite-coated discs with a Netzsch LFA-467 HyperFlash, and the specific heat $C_p(T)$ obtained by comparison with a Pyroceram-9060 standard. The thermal conductivity was then calculated as $\kappa(T) = \rho C_p(T) D(T)$, where ρ is the geometric density corrected by the relative density d_r measured via Archimedes' method (ISO 5017:2013); all specimens exhibited $d_r \geq 97$.

2.3. Active-learning assisted by Bayesian optimisation

In the optimisation stage, active learning assisted by Bayesian optimisation (ALBO) was used to maximise the thermoelectric figure-of-merit zT. A Gaussian-process (GP) regressor acted as a surrogate model that interpolates zT over the discrete domain C spanned by the eleven process variables (see Table 1). At each ALBO iteration the GP was refitted to the current data set and the expected-improvement (EI) acquisition function [33,34] was used to propose a batch of $n_{exp} = 5$ new process conditions, constrained to the domain C, that balance exploration (high predictive uncertainty) and exploitation (high predicted zT). The corresponding GeTe samples were synthesised, processed, and characterised, as described in sections 2.1 and 2.2, and the resulting $(c \in C, zT)$ pairs were appended to the data set before the next iteration.

The initial GP was trained on five randomly chosen set of process parameters, $c_{random} \in C$. All process parameters were scaled to [0,1] with the MinMaxScaler function from the Python package Scikit-learn [35]. Optimisation loops were implemented with the Python package GPyOpt 1.2.0 [36] using default hyper-parameter priors and without additional manual tuning.

The ALBO cycle was terminated when two consecutive iterations produced EI values smaller than 1% of the best observed zT, indicating convergence of the surrogate model.

3. Results and discussion

The initiation of the ALBO process, illustrated in Figure 1b, consisted of five random sets of process conditions constrained within the discretised domain C (see Table 1). The next series of process parameters were proposed via BO with the objective of maximising zT values. Based on these proposals, bulk GeTe samples are synthesised, processed and characterised as depicted in sections 2.1 and 2.2. The process parameters of each sample are listed in Table 1. At each cycle, the results were added to the dataset and the ALBO cycle was repeated until the optimised zT value was achieved. The whole list of concatenated sets of process parameters is available in Table S1.

All samples crystallised in a trigonal cell with space group R3m (#160) as illustrated by PXRD patterns in Figure 2. Consistently with GeTe tendency for Ge vacancies, an impurity identified as cubic elemental Ge is observed in ~71% of the samples. It is worth

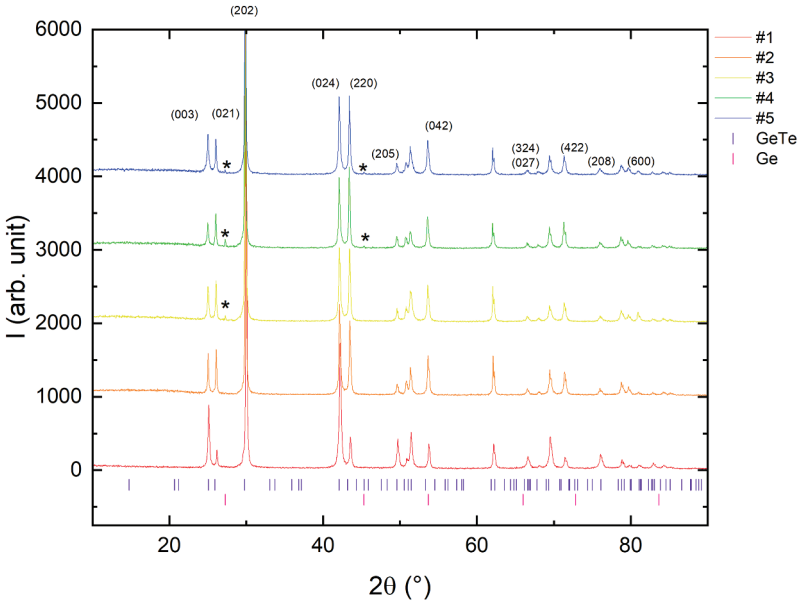

Figure 2. X-ray diffraction patterns for the first cycle associated with the Bragg peak positions of trigonal GeTe (*R3m*) and cubic Ge (*Fd* 3*m*). The * denotes the presence of elemental Ge. All the XRD patterns are available in the SI fi.

mentioning that the detection limit of PXRD prevents the assessment of the presence of the impurity in a very low amount in the other samples. The average lattice parameters calculated from Le Bail refinements, based on the trigonal primitive cell, were $a = 8.331(3)$ Å, and $c = 10.677(3)$ Å, in excellent agreement with previous reports [37]. All the PXRD patterns and Le Bail refinement parameters are available in Figure S1 and Table S2, respectively. The PXRD patterns reveal subtle shifts in peak positions that reflect slight changes in lattice parameters, likely arising from variations in Ge vacancy. As mentioned previously, Ge vacancies are intrinsic to GeTe and form readily due to their low formation energy, significantly altering the electronic structure [38]. They increase hole concentration (p-type carriers), which enhances electrical conductivity but which can also strongly decrease the Seebeck coefficient, S, if not optimally balanced. Simultaneously, these vacancies and Ge phase inclusions introduce phonon scattering centers, which reduce lattice thermal conductivity, included in k with its electronic counterpart, and consequently improve zT. Therefore, differences observed in the PXRD profiles hint at microstructural and defect-level tuning that directly influence thermoelectric properties by modulating carrier transport and thermal conductivity. These subtle crystallographic variations, though chemically minor, can drive substantial performance differences in zT across similarly processed samples.

Figure 3 illustrates the progression of the thermoelectric properties at 700 K across the five ALBO cycles (see Figure S2 for the temperature-dependent properties). The electrical conductivity exhibits a steady increase, reaching approximately 20×10^4 S.m^{-1} for cycle 5, indicating enhanced charge carrier transport. Consistently, the Seebeck coefficient, S, decreases slightly, stabilising around 150 µV.K^{-1}. This inverse relationship between electrical conductivity, s, and S is expected due to the trade-off inherent in optimising thermoelectric materials. The power factor, PF, which combines both properties, shows a slight improvement, narrowing around 4.65 mW.m^{-1}.K^{-2} for cycles 4 and 5 (see Figure S3). The thermal conductivity remains relatively stable, averaging between 3 and 3.5 W.m^{-1}.K^{-1}, with no clear trend emerging over the cycles. Despite the intrinsic measurement uncertainties associated with zT components [39], the figure-of-merit increases rapidly and appears to plateau, as seen in the cycle-averaged zT values (Figure 3f). The accompanying drop in standard deviation is expected due to the progressive saturation of BO-generated suggestions, although its precise origin remains under investigation. Overall, the average zT value rises by approximately 18%, from 0.86 to 1.01, demonstrating the effectiveness of the ALBO methodology. This suggests that, on average, the optimisation primarily enhances electronic transport properties rather than phonon scattering. Given that one of the main common strategies for improving thermoelectric materials typically involves either increasing the Seebeck coefficient (due to its quadratic impact on the power factor) or reducing the thermal

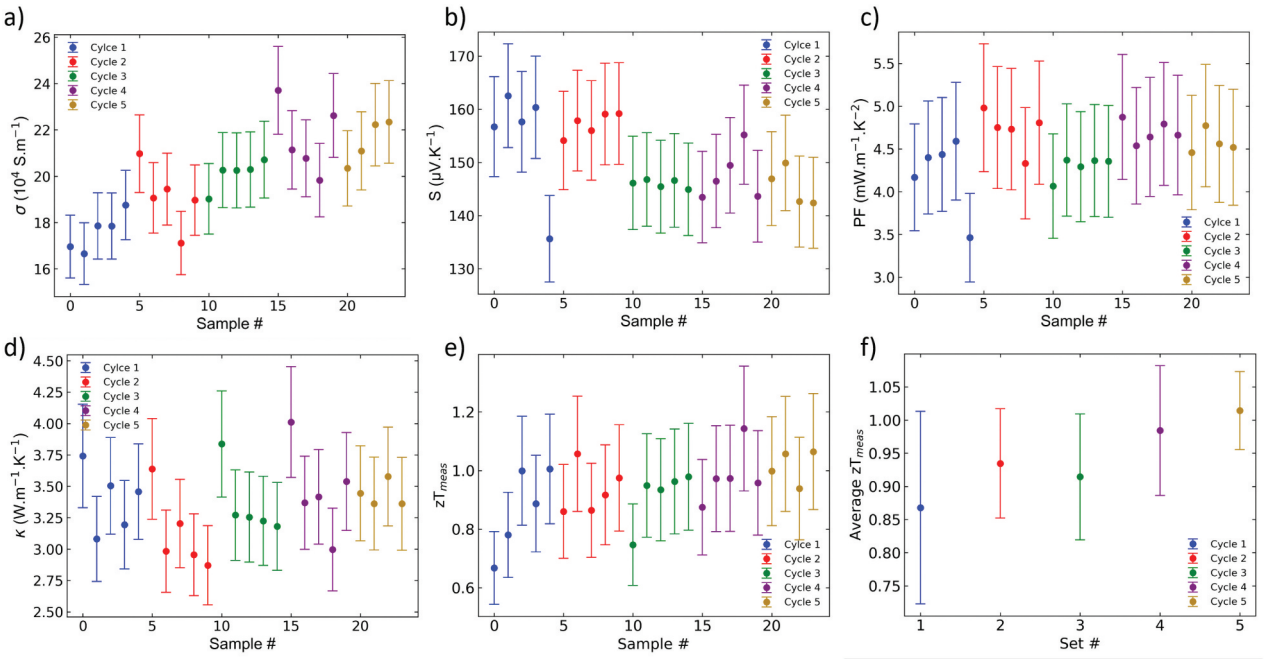

Figure 3. a-e) values of the thermoelectric properties at 700 K as a function of the number of samples along the cycles. The error bars represent the systematic error [39]. f) average of the measured zT values as function of the number of cycles. The error bars represent the standard deviation for each cycle. Figures of the average of the other properties are available in SI.

conductivity, this result is somewhat unexpected and should be considered together with the analysis of the influence of the process parameters.

To clarify which of the eleven process parameters mainly impact the zT, we analysed the final GP surrogate (see Figure S4) with a model-agnostic permutation importance test (Python package Scikit-learn [35]). In brief, the values of one parameter are randomly shuffled (permuted) while all others are kept unchanged; the surrogate is then asked to predict zT for this corrupted data set. The larger the drop in predictive coefficient of determination R^2, the more the model must have relied on that parameter. Because each variable is perturbed independently, permutation importance cleanly disentangles the dense web of correlations that might exist in an eleven-dimensional process space and ranks the parameters on a single, comparable scale. The resulting hierarchy is shown in Figure 4, with the partial dependence plots of zT relative to each of the process parameters individually are shown in Figure S5 and S6. The ranking by permutation importance is unambiguous. The melt-cooling rate *cooling_rate* is, by a wide margin, the single most influential variable. Roughly half as powerful is the melt dwell time $t_{duration}$, followed closely by the initial annealing temperature $T_{annealing}$ and the uniaxial pressure P applied during SPS. A second tier, comprising ball-milling time, the melt heating rate, the SPS annealing temperature, the SPS heating rate and the SPS dwell time, exerts a noticeable but clearly smaller effect. Finally, powder mass and the SPS cooling rate alter the predicted zT only marginally within the ranges explored.

From a chemistry viewpoint, this ranking makes intuitive sense. Fast quenching locks-in a high concentration of Ge vacancies that set the hole density; the duration of the high-temperature melt stage determines how far those vacancies can re-equilibrate before the quench; and the annealing temperature fixes the defect-equilibrium ceiling itself. During densification, the axial pressure chiefly controls porosity and grain-boundary density, feeding directly into both electronic and lattice transport. Down-stream parameters, milling time, heating ramps, secondary SPS factors, fine-tune grain size or defect mobility but cannot rival the dominant levers above.

In short, permutation importance quantifies and rationalises the empirical observation that pristine GeTe performance is governed first by how quickly, how long and at what temperature the melt is cooled, and only secondarily by the details of the subsequent SPS schedule.

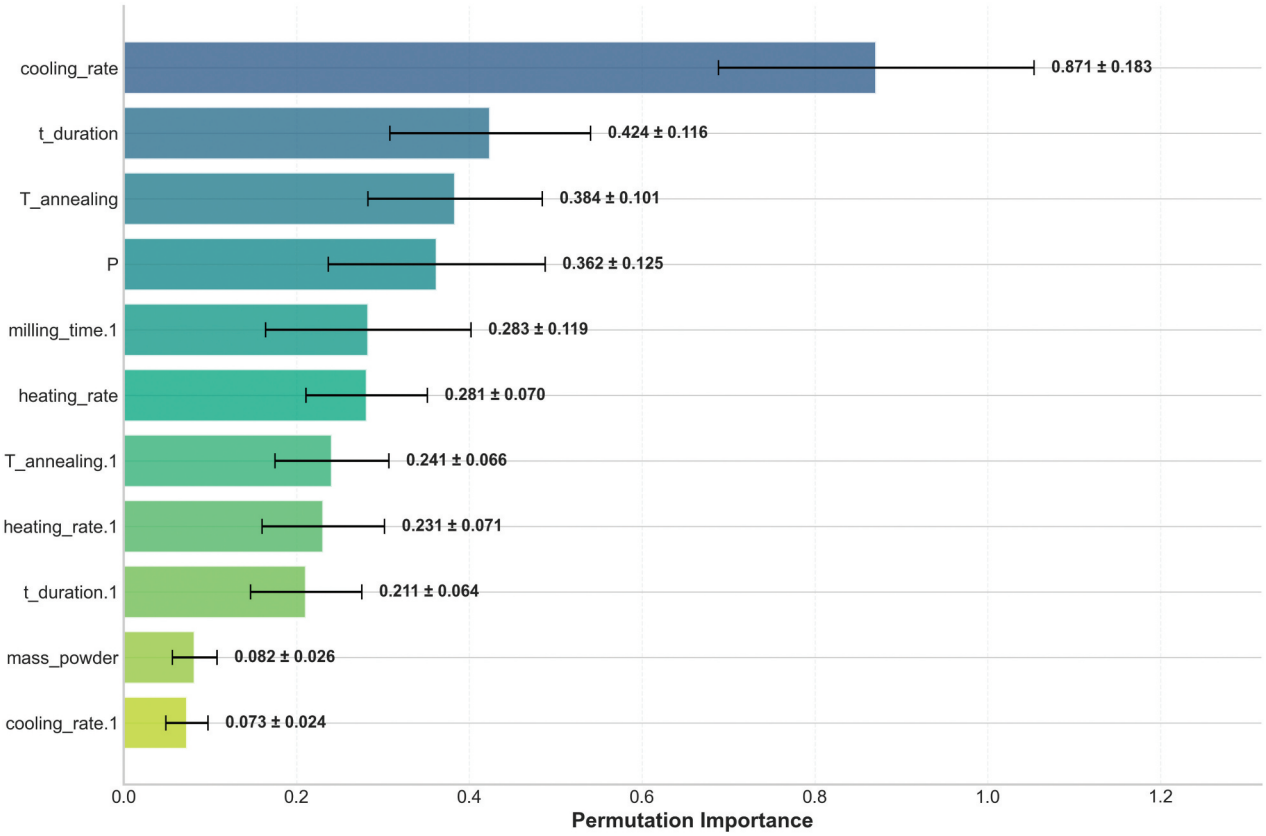

Figure 4. Permutation importance ranking of the 11 process parameters for the GP-fitted zT at 700 K. The parameters are sorted by their importance, with the most important one at the top. The horizontal error bars represent the mean standard deviation on the importances after 30 random permutations for each process parameter.

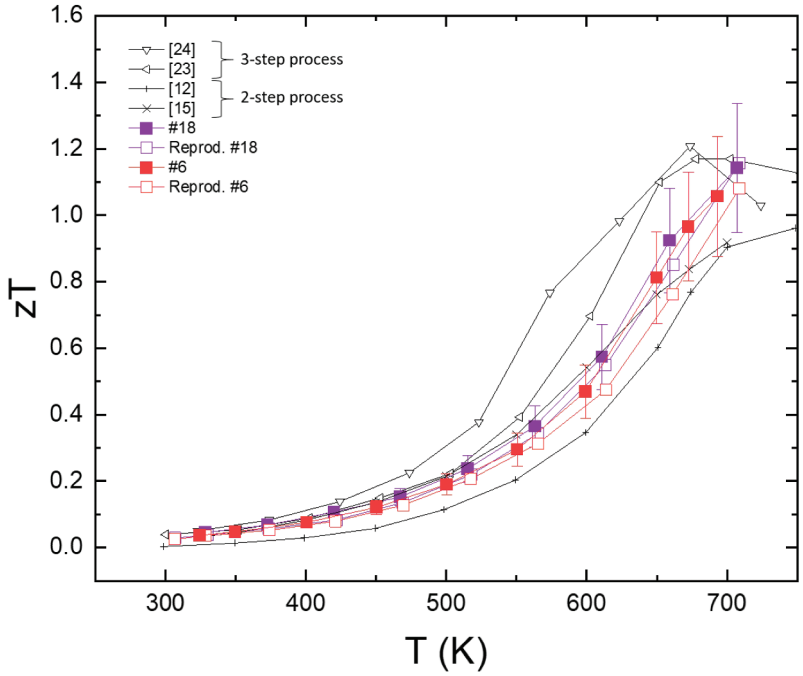

Figure 5. Reproducibility of the two best *zT* values (squares) along with references of the 3-step process (triangles) and 2-step process (crosses). The zT values at ~ 700 K for #18, Reprod.#18 and #6, Reprod.#6 are 1.14, 1.16, and 1.06, 1.08, respectively.

Additionally, comparing from sample to sample, the figure-of-merit *zT* shows a substantial increase, with values ranging from 0.67 in cycle 1 (#0) to 1.14 in cycle 4 (#18), marking a 70% improvement. The sets of process parameters of the two samples with the highest *zT* value (#6 and #18) were used in subsequent syntheses to evaluate the reproducibility of the figure-of-merit. They were successfully reproduced, ensuring the reliability of the 2-step process and of the optimisation approach (Figure 5). At an equivalent 2-step process, involving annealing and densification, the highest *zT* values reported at 700 K for pristine GeTe are around 0.90 [13,16]. In contrast, with a 3-step process that includes an additional 3-day [25] or 5-day [24] annealing, the highest *zT* value reaches approximately 1.20. The detailed study of potential defects, second-phase inclusions, Ge vacancy level, nanostructuration in the best samples is the topic of a second article focused on chemical aspects. Therefore, the ALBO-based methodology we used for optimising all process parameters enables an improvement of *zT* by about 25% over the equivalent 2-step process, and achieves nearly the same efficiency as a 3-step process (within 5%), while drastically reducing process time by over 90% (considering the extra 3-day annealing), and the cost through energy-savings. Overall, the present ALBO-based approach proves to be highly effective into dealing with complex relationships, which are intuitively challenging to grasp, and into achieving a targeted objective, i.e. here, the enhancement of *zT* of an undoped GeTe.

4. Conclusion

This study has demonstrated the efficiency of the application of an active learning pipeline coupled to Bayesian optimisation, ALBO, as a guiding approach to identify the optimal set of parameters for the synthesis and process of pristine GeTe together with an enhanced thermoelectric efficiency. On average, the targeted property *zT* was increased by 18%, from 0.86 to 1.01 between cycle 1 and cycle 5 of ALBO, respectively, illustrating the incremental improvement from cycle to cycle. More specifically, this approach allowed the discovery of a set of process parameters leading to a very efficient thermoelectric pristine GeTe. Indeed, a high *zT* value of 1.14 can be achieved through the 2-step process, comparable to values generally obtained from a more time-consuming 3-step process, which would require an additional 72-hour annealing step. Interestingly, this AL-driven approach thus accelerates the process by a factor of 14 at least, with nearly identical performance (within 5%). The ability to achieve a 25% improvement over similar 2-step process with only 24 experiments, out of more than ~18.2 billion possible parameter combinations, underscores the substantial potential of this method in saving time, energy, and costs. Moreover, this approach effectively navigates the extremely large process parameters space, concomitantly with the complexity of the complex relationships between process parameters and desired material properties, retrieving evidence of

the most influential parameters. Overall, the application of an ALBO methodology offers a powerful and efficient strategy for optimising performance in materials. Notably, this data-driven strategy, developed here for thermoelectric pristine GeTe as a typical example, is versatile enough to be applied to any kind of materials process.

Acknowledgements

F. P. and L. A. thank the Japanese Society for the Promotion of Science (JSPS) for research fellowships. M. H. and A. B. thanks CNRS and NIMS for an undergraduate student internship financial support, respectively. T.M. thanks support from JST Mirai Program (JPMJMI19A1). The authors acknowledge the Material Analysis Station (NIMS, Japan) for the use of the XRD platform. F. P thanks Dr. T. Barbier and Prof. F. Gascoin for helpful discussions.

Disclosure statement

No potential conflict of interest was reported by the author(s).

Funding

JSPS (grants PE20752 and P23705 (F. P.) and 22KF0390 (L. A.)), CNRS and NIMS (M. H. and A. B.).

ORCID

Florent Pawula http://orcid.org/0000-0002-2641-0521

References

[1] Chattopadhyay T, Boucherle JX. Neutron diffraction study on the structural phase transition in GeTe. J Phys C: Solid State Phys. 1987;20(10):1431–1440. doi: 10.1088/0022-3719/20/10/012

[2] Li J, Chen Z, Zhang X, et al. Electronic origin of the high thermoelectric performance of GeTe among the *p*-type group IV monotellurides. NPG Asia Mater. 2017;9(3):e353. doi: 10.1038/am.2017.8

[3] Chen H, Song Q, Zhang Z, et al. Anisotropic thermoelectric properties of GeTe single crystals. J Mater Chem A. 2024;12(18):10974–10983. doi: 10.1039/D4TA01087F

[4] Li J, Zhang X, Lin S, et al. Realizing the high thermoelectric performance of GeTe by Sb-doping and Se-alloying. Chem Mater. 2017;29(2):605–611. doi: 10.1021/acs.chemmater.6b04066

[5] Shuai J, Tan X, Guo Q, et al. Enhanced thermoelectric performance through crystal field engineering in transition-metal-doped GeTe. Mater Today Phys. 2019;9:100094. doi: 10.1016/j.mtphys.2019.100094

[6] Ding G, Gao G, Yao K. High-efficient thermoelectric materials: the case of orthorhombic IV-VI compounds. Sci Rep. 2015;5(1):9567. doi: 10.1038/srep09567

[7] Tang S, Dresselhaus MS. Building the principle of thermoelectric ZT enhancement. arXiv. 2014. doi: 10.48550/arXiv.1406.1842

[8] Allen T, Graser J, Issa R, et al. Machine learning predictions of low thermal conductivity: comparing $TaVO_5$ and $GdTaO_4$. ChemRxiv. 2023. doi: 10.26434/chemrxiv-2023-444s3

[9] Armida SA, Ebrahimibagha D, Ray M, et al. Assessing thermoelectric performance of quasi 0D carbon and polyaniline nanocomposites using machine learning. Adv Compos Mater. 2023;33(3):388–410. doi: 10.1080/09243046.2023.2262875

[10] Packwood D. Bayesian optimization for materials science. Singapore: Springer; 2017.

[11] Lookman T, Balachandran PV, Xue D, et al. Active learning in materials science with emphasis on adaptive sampling using uncertainties for targeted design. Npj Comput Mater. 2019;5(1):21. doi: 10.1038/s41524-019-0153-8

[12] Gelbstein Y, Dado B, Ben-Yehuda O, et al. Highly efficient Ge-rich $Ge_xPb_{1-x}Te$ thermoelectric alloys. J Electron Mater. 2010;39(9):2049–2052. doi: 10.1007/s11664-009-1012-z

[13] Kumar A, Bhumla P, Parashchuk T, et al. Engineering electronic structure and lattice dynamics to achieve enhanced thermoelectric performance of Mn-Sb co-doped GeTe. Chem Mater. 2021;33(10):3611–3620. doi: 10.1021/acs.chemmater.1c00331

[14] Srinivasan B, Boussard-Plèdel C, Bureau B, et al. Thermoelectric performance of codoped (Bi, In)-GeTe and (Ag, In, Sb)-SnTe materials processed by spark plasma sintering. Mater Lett. 2018;230:191–194. doi: 10.1016/j.matlet.2018.07.132

[15] Srinivasan B, Gellé A, Halet J-F, et al. Detrimental effects of doping Al and Ba on the thermoelectric performance of GeTe. Materials. 2018;11(11):2237. doi: 10.3390/ma11112237

[16] Srinivasan B, Gellé A, Gucci F, et al. Realizing a stable high thermoelectric $zT \approx 2$ over a broad temperature range in Ge_{1-x-y} Ga_xSb_y Te via band engineering and hybrid flash-S. Inorg Chem Front. 2019;6(1):63–73. doi: 10.1039/C8QI00703A

[17] Srinivasan B, Le Tonquesse S, Gellé A, et al. Screening of various elements as potential effective dopants for thermoelectric GeTe - an experimental and theoretical appraisal. J Mater Chem A. 2020;8(38):19805–19821. doi: 10.1039/D0TA06710E

[18] Perumal S, Samanta M, Ghosh T, et al. Realization of high thermoelectric figure of merit in GeTe by complementary Bi and in Co-doping. Joule. 2019;3(10):2565–2580. doi: 10.1016/j.joule.2019.08.017

[19] Hong M, Chen Z, Yang L, et al. Realizing zT of 2.3 in $Ge_{1-x-y}Sb_xIn_yTe$ via reducing the phase-transition temperature and introducing resonant energy doping. Adv Mater. 2018;30(11):1705942. doi: 10.1002/adma.201705942

[20] Hong M, Wang Y, Feng T, et al. Strong phonon-phonon interactions securing extraordinary thermoelectric $Ge_{1-x}Sb_xTe$ with Zn-alloying-induced band alignment. J Am Chem Soc. 2019;141(4):1742–1748. doi: 10.1021/jacs.8b12624

[21] Hong M, Lyv W, Li M, et al. Rashba effect maximizes thermoelectric performance of GeTe derivatives. Joule. 2020;4(9):2030–2043. doi: 10.1016/j.joule.2020.07.021

[22] Shuai J, Sun Y, Tan X, et al. Manipulating the Ge vacancies and Ge precipitates through Cr doping for realizing high-performance GeTe thermoelectric.

Small. 2020;16(13):1906921. doi: 10.1002/smll.201906921

[23] Liu Z, Gao W, Zhang W, et al. High power factor and enhanced thermoelectric performance in Sc and Bi co-doped GeTe: hidden role of rhombohedral distortion. Adv Energy Mater. 2020;10(42):2002588. doi: 10.1002/aenm.202002588

[24] Xing T, Zhu C, Song Q, et al. Realizing high-efficiency thermoelectricity in GeTe through synergetic band engineering and nanostructuring. Adv Mater. 2021;33(14):2008773. doi: 10.1002/adma.202008773

[25] Gao W, Liu Z, Zhang W, et al. Improved thermoelectric performance of GeTe via efficient yttrium doping. APL. 2021;118(3):033901. doi: 10.1063/5.0038957

[26] Lambard G, Sasaki TT, Sodeyama K, et al. Optimization of direct extrusion process for Nd-Fe-B magnets using active learning assisted by machine learning and Bayesian optimization. ScrMater. 2022;209:114341. doi: 10.1016/j.scriptamat.2021.114341

[27] Nugraha AS, Lambard G, Na J, et al. Mesoporous trimetallic PtPdAu alloy fi toward enhanced electrocatalytic activity in methanol oxidation: unexpected chemical compositions discovered by Bayesian optimization. J Mater Chem A. 2020;8(27):13532–13540. doi: 10.1039/d0ta04096g

[28] Matsuda S, Lambard G, Sodeyama K. Data-driven automated robotic experiments accelerate discovery of multi-component electrolyte for rechargeable Li-O_2 batteries. Cell Rep Phys Sci. 2022;3(4):100832. doi: 10.1016/j.xcrp.2022.100832

[29] Bourgès C, Lambard G, Sato N, et al. Process optimization on kesterite-based ceramics for enhancing their thermoelectric performances assisted by active machine learning approach. Acta Mater. 2024;281:120342. doi: 10.1016/j.actamat.2024.120342

[30] Zhang H, Xie H. Spark-plasma sintering of thermoelectric materials: a review. Small. 2021;17(13):2006921. doi: 10.1002/smll.202006921

[31] Roisnel T, Rodríguez-Carvajal J. WinPLOTR: a Windows tool for powder diffraction pattern analysis. Mater Sci Forum. 2001;378(381):118–123. https://doi.org/10.4028/www.scientific.net/MSF.378-381.118

[32] Bochmann S, Schilm J, Gas P, et al. Round robin test of Seebeck and electrical resistivity measurements on $CoSb_3$. J Electron Mater. 2018;47:2534–2543. doi: 10.1007/s11664-018-6122-4

[33] Mockus J, Tiesis V, Zilinskas A. The application of Bayesian methods for seeking the extremum. In: Dixon LCW, and Szego GP, editors. Towards global optimisation 2. North-Holland, Amsterdam: North-Holand; 1978. p. 117–129.

[34] Jones DR, Schonlau M. Efficient global optimization of expensive black-box functions. J Global Optim. 1998;13(4):455–492. doi: 10.1023/A:1008306431147

[35] Pedregosa F, Varoquaux G, Gramfort A, et al. Scikit-learn: machine learning in Python. JMLR. 2011;12:2825–2830.

[36] The GPyOpt authors GPyOpt: a Bayesian optimization framework in Python. 2016; Available from: http://github.com/Sheffi

[37] Cheng H, Zhang J, Lin C. Persistence of the R3m phase in powder GeTe at high pressure and high temperature. J Phys Chem C. 2018;122(50):28460–28465. doi: 10.1021/acs.jpcc.8b06511

[38] Edwards AH, Pineda AC, Schultz PA. Theory of persistent, p-type, metallic conduction in c-GeTe. J Phys Condens Matter. 2005;17(32):L329–L335. doi: 10.1088/0953-8984/17/32/L01

[39] Alleno E, Bérardan D, Byl C, et al. A round robin test of the uncertainty on the measurement of the thermoelectric dimensionless fi of merit of $Co_{0.97}Ni_{0.03}Sb_3$. Rev Sci Instrum. 2015;86(1):011301. doi: 10.1063/1.4905250